Copyright © 2013 American Scientific Publishers
All rights reserved
Printed in the United States of America

Journal of Nanoscience and Nanotechnology
Vol. 13, 1–8, 2013

X-Ray Reflectivity Analysis of Titanium Dioxide Thin Films Grown by Cathodic Arc Deposition

A. Kleiman[1,2], D. G. Lamas[1,3], A. F. Craievich[4], and A. Márquez[1,2,*]

[1] *Consejo Nacional de Investigaciones Científicas y Técnicas (CONICET), Argentina*
[2] *Instituto de Física del Plasma (INFIP), CONICET-Universidad de Buenos Aires, Ciudad Universitaria, Pabellón I, C1428EHA Buenos Aires, Argentina*
[3] *Facultad de Ingeniería, Laboratorio de Caracterización de Materiales, Universidad Nacional del Comahue, Buenos Aires 1400, Q8300IBX Neuquén, Argentina*
[4] *Instituto de Física, Universidade de São Paulo, Cidade Universitaria, Travessa R da Rua do Matão, No. 187, 05508-900 São Paulo, Brazil*

TiO_2 thin films deposited by a vacuum arc on a glass substrate were characterized by X-ray reflectivity (XRR), X-ray diffraction (XRD), scanning electron microscopy (SEM) and atomic force microscopy (AFM). Several thin films with different amounts of deposited TiO_2 mass and different deposition and annealing temperatures were studied. A qualitative analysis of the XRD patterns indicated the presence of the anatase and/or rutile crystalline phases in most of the studied samples. From the analysis of the experimental XRR curves—which exhibited a wide angular range of oscillatory behavior—the thickness, mass density and interface roughness were determined. All XRR patterns were well fitted by modeled curves that assume the presence of a single and homogeneous TiO_2 layer over which a very thin H_2O layer is adsorbed. The thickest H_2O adsorption layers were developed in films with the highest anatase content. Our overall results of the XRR analyses are consistent with those derived from the imaging techniques (SEM and AFM).

Keywords: TiO_2, Thin Films, Cathodic Arc Deposition, X-Ray Reflectivity.

RESEARCH ARTICLE

1. INTRODUCTION

Titanium dioxide (TiO_2) thin films were widely studied because of their variety of potential applications, such as the production of hydrogen or electrical energy in solar cells, photo-assisted degradation of pollutants in wastewater,[1,2] gas sensors,[3,4] optical coatings and biomaterials. These films have been produced by using several techniques, such as sol–gel processes[5,6] and sputtering discharges.[7,8]

Cathodic arc deposition (CAD) has demonstrated to be a suitable technique for the synthesis of TiO_2 thin films leading to a high deposition rate and a high adhesion to the substrate.[9] In the CAD process, metallic ions are ejected from the cathode surface and produce a plasma jet characterized by a high ionization degree and also high kinetic ion energy.[10] In this way, metallic coatings can be obtained by placing a substrate facing the plasma jet, while the production of compound films is achieved under reactive neutral gas flowing into the discharge chamber.

The structural features of the films produced by CAD depend on the temperature and bias condition of the substrate during the coating process.[11,12] The main drawback of CAD is that, together with the plasma jet, a few macro-particles are emitted by the cathode. The presence of macro-particles in the coatings produces protuberances and depressions on the film external surface. This effect not only increases the film roughness, but also can degrade mechanical, electrical and optical properties of the coatings. Different filter devices were developed in order to suppress these particles from the ion beam. Descriptions of filters and their functional principles were reported in several works.[13–15]

Employing the CAD technique and using glass substrates placed on a grounded holder, amorphous TiO_2 films were obtained at temperatures lower than 300 °C, while crystalline anatase films were produced when the grounded holder was maintained at higher temperatures, from 300 to 400 °C. Above 400 °C rutile phase was also detected. Amorphous films were crystallized in the anatase phase by annealing at 400 °C for 1 hour, while the rutile phase was also observed when the annealing temperature was 500 °C.[11,16]

*Author to whom correspondence should be addressed.

 1533-4880/2013/13/001/008 doi:10.1166/jnn.2013.8017

In a previous experiment, anatase films deposited by CAD at 400 °C exhibited a good photocatalytic activity in Cr(VI) reduction, the reaction efficiency being increased by increasing the film thickness.[9] Those studies were performed on films with thicknesses varying from 70 up to 700 nm, assuming that the deposited material was in all cases homogeneously distributed along the whole depth, independently of the discharge duration and pulse number.

This work aims at studying the structural features—thickness, density and interface roughness—of TiO_2 thin films grown by the unfiltered CAD technique on glass substrates at different temperatures. The films were characterized by X-ray reflectivity (XRR), X-ray diffraction (XRD), scanning electron microscopy (SEM) and atomic force microscopy (AFM).

2. EXPERIMENTAL PROCEDURE

2.1. Sample Preparation

The DC vacuum arc device used in this work was previously described.[17] The arc was established between a 55 mm diameter titanium cathode and the anodic vacuum chamber. The experiment was carried out under a discharge current of 130 A. The base pressure of the system was below 10^{-2} Pa. An oxygen flow was added to the chamber during the discharge while the pressure was continuously monitored with a Pirani manometer. The gas flow was kept at 40 sccm and the pressure at ~ 3 Pa during the whole growth process. In order to obtain thin films with different thicknesses the deposition time was varied for each of them from 0.5 to 5 min. The discharges were performed at 1 min intervals to prevent an overheating of the device. 2.8×2.9 cm^2 nearly square glass substrates were placed along the chamber axis at 26 cm from the cathode and mounted on a grounded heater. The films were deposited on glass substrates kept at room temperature or at (400 ± 40) °C. Samples obtained at room temperature were annealed at 400 °C in air during 1 h.

Five TiO_2 thin films prepared under different conditions were studied by XRD and XRR. The differences between the growth processes are differences in amount of deposited mass (DM), deposition temperature (DT) and further annealing temperature (AT). The deposited masses were approximately 0.2, 0.3, 0.4, 0.5 and 0.6 mg for samples labeled as A, B, C, D and E, respectively. The values of the other preparation parameters are reported in Table I.

Table I. Preparation parameters for the different samples.

Sample label	DM (mg)	DT (°C)	AT (°C)
A	0.2	400	600
B	0.3	400	–
C	0.4	400	–
D	0.5	400	–
E	0.6	20	400

2.2. Structural Characterization

The surface morphology of the grown thin films was studied by SEM using a Philips 515 microscope and by AFM using a Nanoscope III Digital-VEECO microscope operated in tapping mode. The depth profile of the films was also studied by SEM (Zeiss Supra 40).

The crystalline phases in the films were identified by glancing-angle XRD using a Philips PW 3710 diffractometer equipped with thin film attachment, with CuK$_\alpha$ radiation ($\lambda = 0.15418$ nm). The angle of incidence was set at 1° (fixed during the whole diffractogram) and a divergence slit of (1/12)° was used. Because of probable strong effects of preferred crystal orientation on the intensity of XRD peaks, no quantitative determinations of the fraction of phases were carried out.

The XRR technique allows for the quantitative determination of relevant structural parameters of thin films, namely density, thickness and roughness of air/film and film/substrate interfaces.[18] The refractive index, n, of any material for X-rays is slightly lower than unity and can be written as:[19]

$$n = 1 - \delta - i\beta \tag{1}$$

with

$$\delta = (\lambda^2/2\pi) r_e N_A \rho (Z + f')/A \tag{2}$$

and

$$\beta = \delta f''/(Z + f') \tag{3}$$

δ and β being the dispersion and absorption terms, respectively, ρ the mass density, λ the X-ray wavelength, r_e the classical electron radius, N_A the Avogadro's number, A the atomic mass, Z the atomic number, and the factors f' and f'' the real and imaginary parts of the atomic scattering factor corrections, respectively.[20] The parameters A and Z refer to the basic atomic group (i.e., TiO_2 in the present study).

For angles of incidence—with respect to the surface—smaller than a certain critical angle, θ_c, the incident X-ray beam is totally reflected on the film surface, while for angles higher than θ_c the radiation partially penetrates into the film. Thus, the reflected X-ray intensity is unity at very small angles, exhibits a more or less sharp decrease at the critical angle θ_c, and shows an oscillatory pattern above θ_c. The angular positions of interference maxima and minima depend on film thickness d. For single layer thin films, θ_c and d are related through a modified Bragg equation:[21]

$$\theta_m^2 = \theta_c^2 + (m + \Delta m)^2 (\lambda/2d)^2 \tag{4}$$

where θ_m are the angles of the interference extremes (maxima and minima), m refers to the interference order and Δm are parameters taking the values $\Delta m = 0$ for minima and $\Delta m = 1/2$ for maxima. On the other hand, the critical

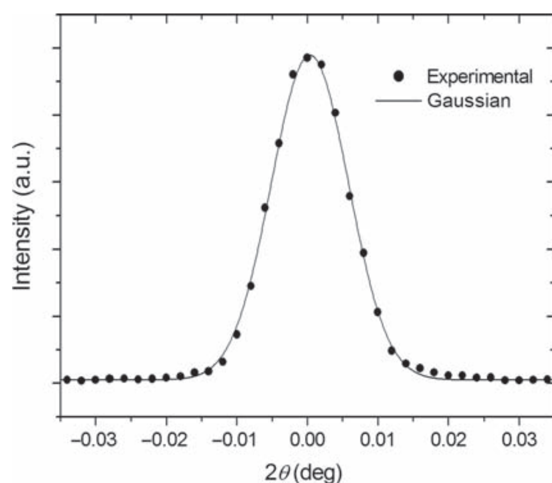

Fig. 1. Profile of the incident X-ray beam measured at an angle $\theta = 0$.

angle can be related to the refractive index from the Snell law. For very small angles we have

$$\theta_c^2 \approx 2\delta \tag{5}$$

By coupling Eqs. (2) and (5) the mass density, ρ, of the thin films can be directly determined from the simple measurement of the critical angle for total reflection, θ_c.

X-ray reflectivity measurements were performed by using the D12A-XRD1 and D10A-XRD2 beamlines of the National Synchrotron Light Source (LNLS), Campinas, Brazil. The energy of the X-rays was 8 keV (λ = 0.1549 nm) and the opening of the slit that defines the vertical size of the incident X-ray beam was 50 μm. The angle of incidence with respect to the surface, θ, was varied from 0.1° to 1.5° by a θ(sample)–2θ(detector) scanning procedure.

Smearing effects of the XRR intensity curves mainly depend on the width of the incident beam, the opening of the receiving (detector) slit and on the macroscopic deviations of the surface from a perfect flatness.[22] In this experiment, the overall smearing effect was evaluated from the profile of the reflected beam while keeping the angle of incidence θ fixed at a given value lower than θ_c and sweeping the detector 2θ angles around the expected angle for total reflection. Figure 1 displays a typical X-ray beam profile for $\theta = 0$. The measured profile is a Gaussian function that exhibits a half maximum width $\Delta(2\theta)$ equal to 0.011°. The widths of the Gaussians for the alignment conditions corresponding to the different studied samples were similar.

3. EXPERIMENTAL RESULTS

3.1. Microscopy

The typical surface morphology of thin films grown at 400 °C is shown in Figure 2. A SEM image from the film surface is presented in Figure 2(a) in which a uniform base with a few macro-particles, commonly observed in thin films grown by unfiltered-CAD, can be noticed. Figure 2(b) displays an AFM image corresponding to the same sample over an area without macro-particles, in which a surface composed of columnar grains, rather dense and without voids is apparent. The columnar structure is also revealed in a SEM cross section image displayed in

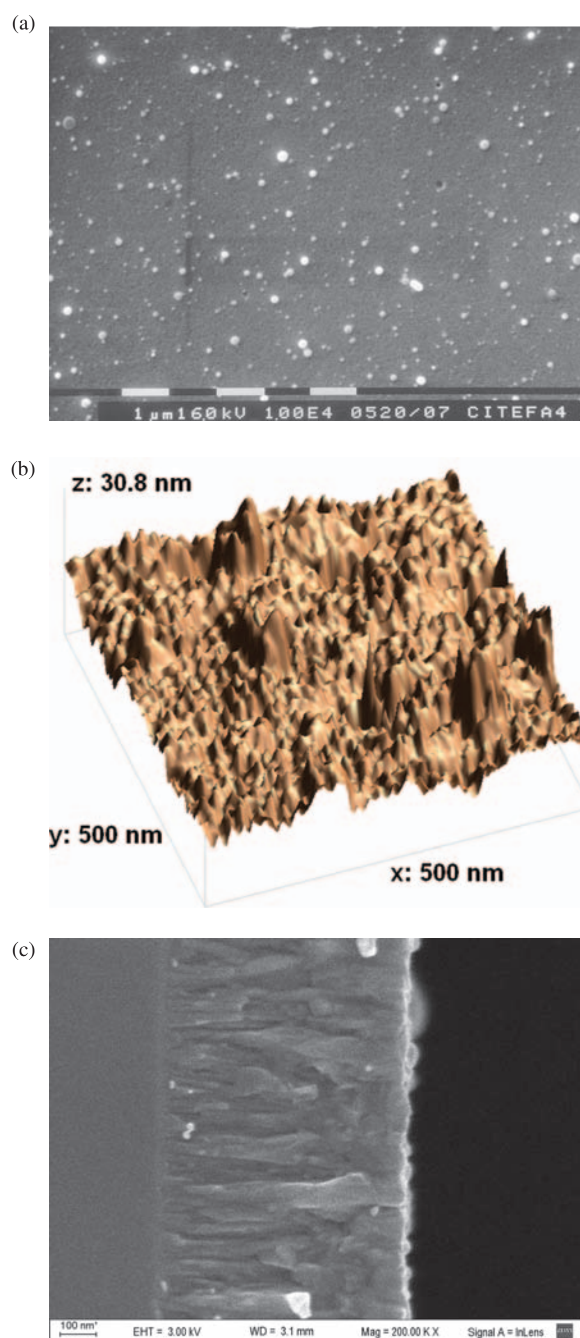

Fig. 2. Typical structure of anatase thin films grown at 400 °C; (a) SEM and (b) AFM images from the film surface, (c) SEM image from the cross section depth profile.

RESEARCH ARTICLE

Figure 2(c), in which a quite uniform and homogeneous profile is observed. The image in Figure 2(c) corresponds to a film thicker than the films studied by XRR, showing more clearly the depth profile. Samples grown at room temperature, annealed at 400 °C, exhibit a similar structure containing higher sized columns.

3.2. X-Ray Diffraction

The XRD patterns of the five studied TiO_2 thin films are plotted in Figure 3. They correspond to the series of studied samples labeled as A, B, C, D and E, with increasing amounts of deposited mass. In this figure the angular positions of the Bragg peaks expected for the crystalline phases that are often exhibited by TiO_2, i.e., anatase and rutile, are also indicated. In the diffractograms corresponding to samples B, C, D and E, the presence of several Bragg peaks has been noticed corresponding to anatase and/or rutile crystalline phases and a broad halo in the 2θ range from 20 to 40°. For this angular range the X-ray penetration in TiO_2 is expected to be of about 0.3 μm, value much higher than the thicknesses of all the studied TiO_2 thin films, as we will see below. Thus we could safely conclude that the broad halo observed in all XRD patterns is related to the diffuse scattering produced by the amorphous structure of the glass substrate.

The diffractogram corresponding to the sample with the highest deposited mass (sample E, DM = 0.6 mg), grown at room temperature and then annealed at 400 °C, exhibits the presence of strong and well defined Bragg peaks corresponding to the anatase phase.

On the other hand, the XRD patterns corresponding to thin films grown at 400 °C without further annealing containing intermediate amounts of deposited mass (samples B, C and D with DM = 0.3, 0.4 and 0.5 mg, respectively) exhibit several Bragg peaks indicating the presence of the anatase and/or rutile phases. The intensity ratios of the Bragg peaks corresponding to these phases are very different for each diffractogram of this set. We did not try to quantitatively determine the volume fractions of anatase and rutile phases from these different ratios because significant differences in peak intensities may be due to different preferred orientations or differences in crystallite size, effects not investigated in this work.

In the XRD pattern corresponding to the thin film with the lowest amount of mass deposited at 400 °C (sample A, DM = 0.2 mg) the presence of any Bragg peak could be identified, neither those of anatase nor those of rutile. In this pattern only a broad XRD halo produced by the glass substrate is apparent. This thin film (sample A) was further submitted to an additional annealing process at 600 °C (in air, during 1 h) to favor the formation of a crystalline structure. However, even after applying this additional annealing, no Bragg peaks were detected. In Section 4 we will discuss the a priori unexpected difference of this result referring to sample A with respect to those previously reported corresponding to samples B, C and D.

3.3. Determination of Film Thickness and Density from X-Ray Reflectivity Results

The XRR patterns of the five TiO_2 thin films analyzed in this work are plotted in Figure 4. We can notice that after a constant reflectivity (equal to 1) below the critical angle θ_c, a wide angular range exhibiting well defined oscillations are apparent for higher θ angles, for all thin films with different deposited mass. The angular increments between interference maxima and minima are smaller for thin films with higher deposited mass. This

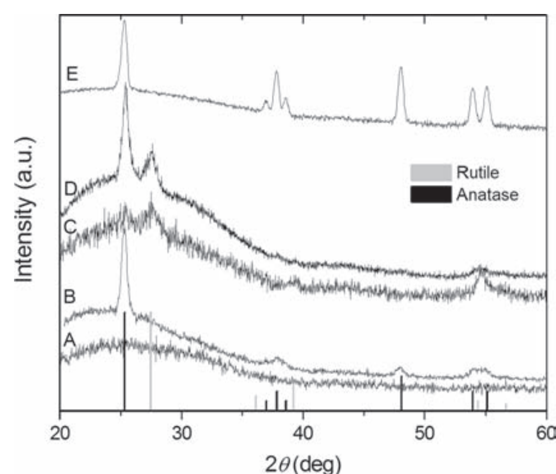

Fig. 3. XRD spectra associated to the five studied TiO_2 thin films. Positions of Bragg peaks corresponding to anatase and rutile are indicated with black and grey bars, respectively. Signals are vertically displaced for clarity.

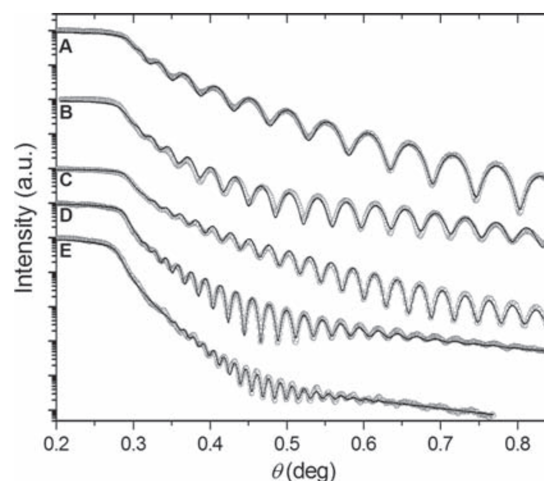

Fig. 4. X-ray reflectivity patterns corresponding to the five studied TiO_2 thin films. Curves are vertically displaced for clarity. The solid lines correspond to the best fit to the experimental curves applying model 2 (see text).

RESEARCH ARTICLE

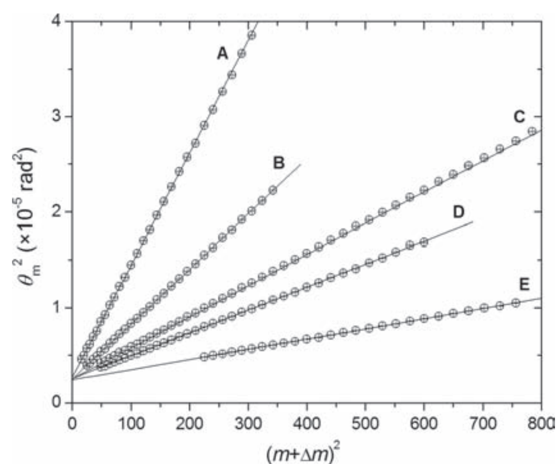

Fig. 5. θ^2 versus $(m+\Delta m)^2$ linear plots. The thickness of the thin film is determined from the slope α as $d = \lambda/(2\alpha^{1/2})$.

feature—as a priori expected—indicates that the thickness of the studied thin films increases for increasing deposited mass.

In order to determine the film thicknesses we have applied the modified Bragg equation (Eq. (4)). For this purpose the squared angles corresponding to maxima and minima were plotted in Figure 5 as functions of $(m+\Delta m)^2$. As predicted by Eq. (4), the results plotted in Figure 5 are in all cases well fitted by straight lines. The thicknesses of the thin films were determined from the slopes, $\alpha = [\lambda/(2d)]^2$, of the straight lines determined by the least square procedure. The mass densities of the films were derived from the critical angles through Eqs. (2) and (5), using $f' = 0.36$ and $f'' = 1.94$ for TiO_2.[20] In turn, the critical angles were determined as the average values between those obtained from the y-intercepts in Figure 5 and from the angles at which the reflected intensities fall to 50%. The structural parameters derived from this procedure (densities and thicknesses) corresponding to all studied thin films are reported in Table II.

3.4. X-Ray Reflectivity Fitting Procedure

The whole XRR curves plotted in Figure 4 were analyzed by applying the Parratt32 v1.6 software. This program simulates the XRR intensity function for a given set of relevant parameters and determines them by the best fitting

Table II. Structural parameters determined from the XRR analysis.

Sample label	ρ (g/cm^3)	d (nm)	σ (nm)	σ_a (nm)	d_a (nm)	σ_s (nm)
A	4.24 ± 0.02	71	2.1	1.1	1	1.4
B	4.01 ± 0.02	102	1.5	1.0	5	1.3
C	4.00 ± 0.04	134	1.7	1.4	2	0.7
D	4.00 ± 0.07	158	3.0	2.4	6	0.2
E	3.79 ± 0.06	237	4.0	3.4	6	0.9

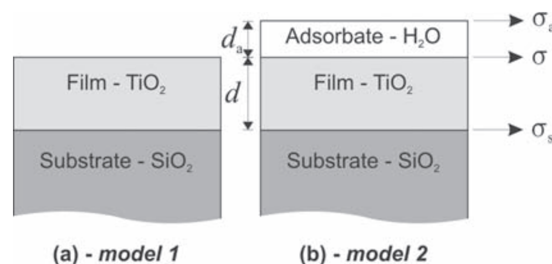

Fig. 6. Thin film models.

procedure. The varying fitting parameters are the thickness, the refractive index—both dispersion and absorption terms—and the roughness (σ). Parratt software can be applied to thin films composed of one or more successive layers on a thick substrate.

The simplest proposed model is drawn in Figure 6(a) (*model* 1). This model consists of a single layered TiO_2 film—with structural parameters d, δ, β and σ—deposited on a thick SiO_2 glass substrate having structural parameters labeled as δ_s, β_s and σ_s. The substrate was assumed to be pure SiO_2 for sake of simplicity because silica is the predominant compound (~70%) in window glasses. Moreover, the density of the glass substrates—estimated from their weight and volume—was close to that of SiO_2 (2.49 g/cm^3).

For all simulations, the roughness parameters σ and σ_s were set as varying parameters, while d and δ were kept constant taking the values determined as described in the previous section. The parameters δ_s and β_s of the substrate were calculated by applying Eqs. (2) and (3), assuming a mass density of 2.49 g/cm^3 and taking f' and f'' for SiO_2 from tables.[20] The absorption parameter β was also allowed to vary, its final value not significantly differing from the initial one, which was initially calculated from the parameter δ by applying Eq. (3).

The simulated pattern that best fit to the experimental XRR curve corresponding to sample C and assuming the simple *model* 1 is displayed in Figures 7(a) ($0 < \theta < 0.8°$) and (b) ($0.8° < \theta < 1.4°$). We can notice in Figure 7 that the best fitted curve (solid line) exhibits (i) noticeable oscillations at very small angles, near $\theta \sim 0.35°$, over which the experimental pattern is smooth, (ii) a few sharp minima over the $0.6° < \theta < 0.7°$ range that are not so pronounced in the experimental pattern, and (iii) a smooth behavior for $\theta > 1.2°$ in contrast to the still oscillatory experimental pattern.

A second attempt was to assume a two-layer model (*model* 2) as schematically shown in Figure 6(b) plus a smearing contribution related to the width of the incident beam and resolution slit and deviations from the flatness of the studied films.[23] Since TiO_2 is a hydrophilic material, we have assumed that a thin layer of adsorbed H_2O (d_a, δ_a, β_a and σ_a) homogeneously covering the TiO_2 thin film could be added. For this second model the Parratt software for two layers was applied. The parameters δ_a and β_a

RESEARCH ARTICLE

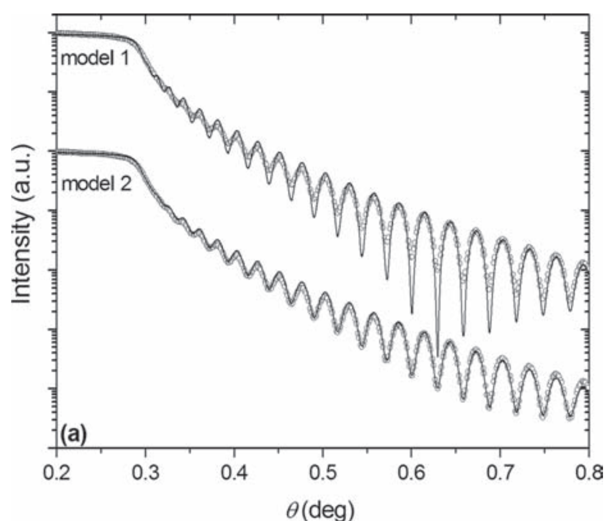

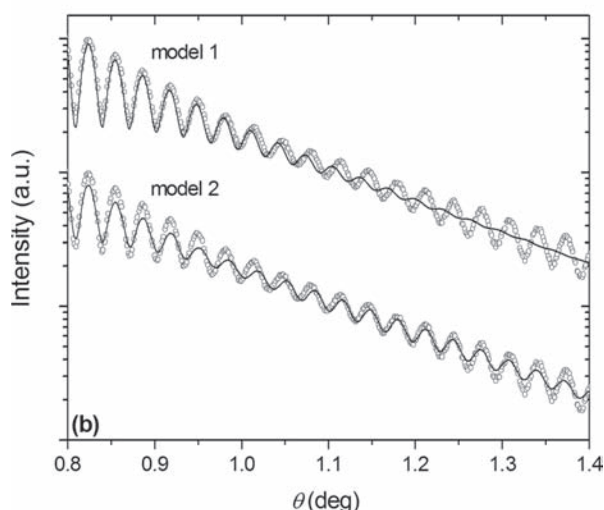

Fig. 7. Experimental XRR data and fitted curves (solid lines) (a) below 0.8°. (b) above 0.8°.

were kept constant and set to the initial values determined by applying Eqs. (2) and (3). The density of H_2O was set equal to 1 g/cm^3. The other parameters d_a and σ_a were allowed to vary together with σ and σ_s. The experimental and best fitted patterns displayed in Figures 7(a) and (b) for *model* 2 demonstrated that the reflectivity curves calculated under the assumption of a two-layer model (TiO_2 thin film + H_2O layer) fit well—and better than the single layer model—to the experimental data over the whole angular range. It is worth mentioning that the only inclusion of the smearing parameter in *model* 1 amended the fit at small angles ($\theta < 0.8°$) but not over the whole studied angle range.

The XRR profiles that best fitted the whole set of experimental patterns corresponding to all the samples studied here are displayed as solid lines in Figure 4 and the parameters derived by the described fitting procedure are reported in Table II.

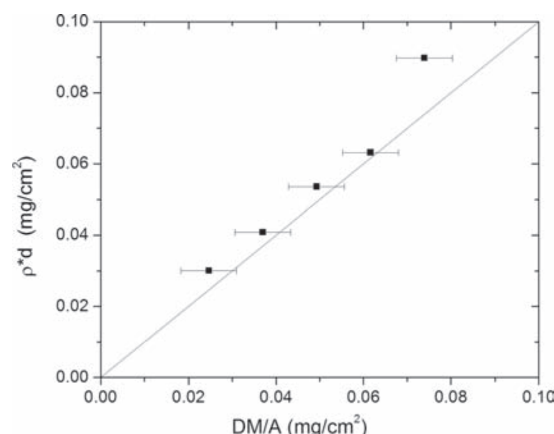

Fig. 8. Specific deposited mass $m_a = \rho \cdot d$—the values of ρ and d being derived from XRR measurements—as a function of the nominal specific deposited mass $m'_a = \text{DM/A}^2$.

4. DISCUSSION

The results reported in Table II indicate that, as expected, the thickness of the thin films increases monotonously as the amount of deposited mass increases. Even though the amount of deposited mass in each sample was determined with a rather low accuracy, we have tried to verify the consistency of the experimental results derived from our XRR measurements. For this purpose we have plotted in Figure 8 the specific amount of deposited mass per unit area $m_a = \rho \cdot d$ (with both parameters, ρ and d, determined from our XRR analysis) as a function of the nominal specific deposited mass, $m'_a = \text{DM/A}$, A being the known surface area of the glass substrate. We can notice in Figue 8 that the experimental values of m_a as function of m'_a lie, considering the uncertainties, in the straight line that is expected under ideal conditions. This result demonstrates the consistent trend of the parameters derived from our XRR analysis.

Taking into account the values of bulk mass density of anatase ($\rho_A = 3.89$ g/cm^3), rutile ($\rho_R = 4.23$ g/cm^3) and amorphous TiO_2 ($\rho_{am} = 3.6$ g/cm^3),[12] we can infer that the densities determined for samples B, C and D—all of them close to 4.00 g/cm^3—are consistent with the presence in these samples of a mixture of anatase and rutile phases. On the other hand, the density of sample E was determined to be equal to 3.79 g/cm^3—i.e., slightly lower than expected for anatase—while its XRD pattern exhibits Bragg peaks corresponding to the anatase phase. Thus both results indicate that sample E is composed of anatase phase.

However XRD and XRR experimental results corresponding to sample A (i.e., the thinnest film) exhibit apparently contradictory features. As a matter of fact, the density of sample A derived from XRR is 4.24 g/cm^3, i.e., very close to the density of rutile (4.23 g/cm^3), while its XRD pattern (Fig. 3) does not exhibit any Bragg peak of crystalline rutile. Since this sample was further annealed at 600 °C the presence of the rutile phase is a priori

RESEARCH ARTICLE

expected.[16] Therefore the observed features of our XRR and XRD results imply that the thinnest film (sample A) contains very small rutile crystals that produce very wide and weak diffraction peaks instead of well-defined and narrow XRD peaks.

The thicknesses of the H_2O layers covering the different films range from 1 to 6 nm, the thickest H_2O layers being formed on the films that exhibit the best defined and strongest anatase peaks in XRD patterns, i.e., samples B, D and E (Fig. 3). This higher thickness of the water adsorption layer developed on anatase is a priori expected because this phase is more hydrophilic than rutile.[24]

The values of the surface roughness of the studied thin films—determined from the fitting procedure and reported in Table II—agreed with previous results obtained by AFM for films grown by CAD (~ 2 nm for films grown at 400 °C and ~ 5 nm for those deposited at room temperature[16]), the roughness of film E being higher than those of the other thin films.

The roughness determined from AFM images referred to areas of the thin films without macro-particles, while those derived from XRR analysis correspond to essentially the whole sample. This result indicates that the average roughness of the surface was not significantly affected by the presence of macro-particles. On the other hand, the roughness of the H_2O layers was similar to that of the corresponding film surface. The roughness values determined for the substrate agreed with the roughness measured with AFM in several regions of the glass (0.6–1.5 nm).

Finally it is worth emphasizing that the assumption of *model* 2 ($TiO_2 + H_2O$ layers) including instrumental smearing effects greatly improved the agreement between the experimental and simulated X-ray reflectivity patterns. However, the relevant structural parameters derived for the film from *model* 2 did not significantly differ from those determined under the hypothesis of *model* 1 (single TiO_2 layer).

5. CONCLUSIONS

Different annealing conditions and amounts of deposited mass lead to the formation of TiO_2 thin films with different structural features. The results of X-ray reflectivity analysis curves indicate that the studied thin films are essentially homogeneous and exhibit a rather low roughness, without any significant influence of macroparticles. The films have thicknesses ranging from 71 up to 237 nm and roughness ranging from 1.5 up to 4 nm.

XRR results indicate that TiO_2 thin films grown at 400 °C without additional annealing (samples B, C, D) exhibit mass densities within the range between the density of anatase (3.89 g/cm^3) and that of rutile (4.24 g/cm^3), thus suggesting that these thin films contain a mixture of both crystalline phases. Our XRD analyses confirm the presence of anatase and/or rutile phases in all samples except in the thinnest film (sample A) even after being annealed at 600 °C.

On the other hand, the density of the thinnest TiO_2 film was determined to be very close to the mass density of the rutile phase, which is expected to be present after a thermal annealing at 600 °C. However, as mentioned above, no well-defined peaks were detected in the XRD pattern. We therefore concluded that the rutile crystals in the thinnest film are very small thus producing very weak peak profiles that could not be identified in the XRD patterns.

In spite of most of the studied thin films were grown by applying several successive deposition steps, an excellent agreement between experimental and simulated XRR curves based on a simple $TiO_2 + H_2O$ model was observed in all cases. This led us to conclude that the grown films are composed of a single and homogeneous TiO_2 layer covered with a very thin layer of adsorbed water, without any other significant structural feature.

Acknowledgments: This work was supported by grants from Universidad de Buenos Aires, CONICET (PIP 11220090100219) and CNPq (PROSUL 490580/2008-4). XRR measurements were performed at LNLS (under proposals 6060-D12A-XRD1-8693 and 6881-D10A-XRD2-10013). Glancing-angle XRD studies were carried out at CINSO, CONICET-CITEDEF (Argentina).

References and Notes

1. M. I. Litter, *Appl. Catal. B-Environ.* 23, 89 (**1999**).
2. M. Kitano, M. Matsuoka, M. Ueshima, and M. Anpo, *Appl. Catal. A-Gen.* 325, 1 (**2007**).
3. N. Savage, B. Chwieroth, A. Ginwalla, B. R. Patton, S. A. Akbar, and P. K. Dutta, *Sens. Actuators, B-Chem.* 79, 17 (**2001**).
4. Z. M. Seeley, A. Bandyopadhyay, and S. Bose, *Mater. Sci. Eng. B* 164, 38 (**2009**).
5. L. Sun, T. An, S. Wan, G. Li, N. Bao, X. Hu, J. Fu, and G. Sheng, *Sep. Purif. Technol.* 68, 83 (**2009**).
6. G. S. Devi, T. Hyodo, Y. Shimizu, and M. Egashira, *Sens. Actuators B-Chem.* 87, 122 (**2002**).
7. O. Zywitzki, T. Modes, H. Sahm, P. Frach, K. Goedicke, and D. Glöß, *Surf. Coat. Technol.* 180/181, 538 (**2004**).
8. C. H. Heo, S. B. Lee, and J. H. Boo, *Thin Solid Films* 475, 183 (**2005**).
9. A. Kleiman, A. Márquez, M. L. Vera, J. M. Meichtry, and M. I. Litter, *Appl. Catal. B-Environ.* 101, 676 (**2011**).
10. R. L. Boxman, D. M. Sanders, and P. J. Martin (eds.), Handbook of Vacuum Arc Science and Technology: Fundamentals and Applications, Noyes Publications, Park Ridge, NJ (**1995**).
11. H. Takikawa, T. Matsui, T. Sakakibara, A. Bendavid, and P. J. Martin, *Thin Solid Films* 348, 145 (**1999**).
12. A. Bendavid, P. J. Martin, and H. Takikawa, *Thin Solid Films* 360, 241 (**2000**).
13. I. I. Aksenov, V. E. Strel'nitskij, V. V. Vasilyev, and D.Y. Zaleskij, *Surf. Coat. Technol.* 163/164, 118 (**2003**).
14. R. L. Boxman and V. N. Zhitomirsky, *Rev. Sci. Instrum.* 77, 021101 (**2006**).
15. A. Kleiman, A. Márquez, and R. L. Boxman, *Plasma Sources Sci. Technol.* 17, 015008 (**2008**).
16. A. Kleiman, A. Márquez, and D. G. Lamas, *Surf. Coat. Technol.* 201, 6358 (**2007**).

RESEARCH ARTICLE

17. A. Márquez, G. Blanco, M. E. Fernandez de Rapp, D. G. Lamas, and R. Tarulla, *Surf. Coat. Technol.* 187, 154 **(2004)**.

18. L. G. Parratt, *Phys. Rev.* 95, 359 **(1954)**.

19. J. Daillant and A. Gibaud, X-Ray and Neutron Reflectivity: Principles and Applications, Springer, Berlin **(1999)**.

20. B. L. Henke, E. M. Gullikson, and J. C. Davis, *At. Data Nucl. Data Tables* 54, 81 **(1993)**.

21. A. Segmüller, *Thin Solid Films* 18, 287 **(1973)**.

22. A. Gibaud, G. Vignaud, and S. K. Sinha, *Acta Cryst. A* 49, 642 **(1993)**.

23. R. J. Matyi, M. S. Hatzistergos, and E. Lifshin, *Thin Solid Films* 515, 1286 **(2006)**.

24. D. Zare-Hossein-Abadi, A. Ershad-Langroudi, A. Rahimi, and S. Afsar, *J. Inorg. Organomet. Polym.* 20, 250 **(2010)**.

Received: 18 January 2013. Accepted: 17 April 2013.